A Comparative Investigation of Prevalent Hydrodynamic Modelling Approaches for Floating OffshoreWind Turbine Foundations: A TetraSpar Case Study

Thomsen, Jonas Bjerg; Têtu, Amélie; Stiesdal, Henrik

Published in:
Journal of Marine Science and Engineering

DOI (link to publication from Publisher):
10.3390/jmse9070683

Publication date:
2021

Document Version
Publisher's PDF, also known as Version of record

Journal of *Marine Science and Engineering*

MDPI

Article

A Comparative Investigation of Prevalent Hydrodynamic Modelling Approaches for Floating Offshore Wind Turbine Foundations: A TetraSpar Case Study

Jonas Bjerg Thomsen [1,*], Amélie Têtu [1] and Henrik Stiesdal [2]

[1] Department of the Built Environment, Aalborg University, Thomas Manns Vej 23, 9220 Aalborg Ø, Denmark; amt@build.aau.dk
[2] Stiesdal Offshore Technologies A/S, Nørrevoldgade 45, 5000 Odense C, Denmark; hst@stiesdal.com
* Correspondence: jbt@build.aau.dk

Abstract: Numerical models have been used extensively in the design process of the TetraSpar floating offshore wind turbine (FOWT) foundation to optimize and investigate the influence from a number of structural and environmental conditions. In traditional offshore design, either the Morison approach or a linear boundary element method (BEM) is applied to investigate the hydrodynamic loads on a structure. The present study investigated and compared these two methods and evaluated their applicability on the TetraSpar FOWT concept. Furthermore, a hybrid model containing load contributions from both approaches was evaluated. This study focuses on motion response. In the evaluation, hydrodynamic data from BEM codes are applied, while the commercial software package OrcaFlex is utilized for time series simulations of the coupled structure. The investigation highlights the difference between the modelling approaches and the importance of particularly drag and inertia contributions. By optimizing the input coefficients, reasonable agreement between the models can be achieved.

Keywords: floating offshore wind turbines; hydrodynamics; OrcaFlex; Morison; boundary element method; numerical simulation; TetraSpar

Citation: Thomsen, J.B.; Têtu, A.; Stiesdal, H. A Comparative Investigation of Prevalent Hydrodynamic Modelling Approaches for Floating Offshore Wind Turbine Foundations: A TetraSpar Case Study. *J. Mar. Sci. Eng.* **2021**, *9*, 683. https://doi.org/10.3390/jmse9070683

Academic Editor: Rodolfo Trentin Gonçalves

Received: 10 May 2021
Accepted: 15 June 2021
Published: 22 June 2021

1. Introduction

The wind energy sector is in continuous development and today, both offshore and onshore wind have become commercially viable alternatives to conventional power generation. With increasing world-wide energy consumption, focus on climate change, and many countries' energy policies, the desire to expand the offshore wind energy sector is particularly eminent and considered necessary to reach the climate goals [1–4]. In 2018, the European Commission stated that Europe would need between 230 and 450 GW of offshore wind power by 2050, with 450 GW corresponding to 30% of Europe's expected electricity demand [3]. Consequently, more wind energy farms need to be developed, however, many of the offshore sites with the highest available wind energy resource and the lowest levelized cost of energy (LCoE), are inaccessible to the conventional bottom-fixed turbines, as the economical feasibility becomes undesirably low when reaching water depths of ~50 m [5,6]. As a consequence, recent years have seen an extensive focus on the development of floating offshore wind turbine (FOWT) technologies. When utilizing floating foundations, water depths no longer form a limiting factor in selecting feasible wind energy sites. For countries like, e.g., Norway, where most offshore wind sites are limited by deep water depths, the floating technology currently forms a paramount potential for expanding the renewable energy sector and tap further into the wind energy potential. Similar considerations can be made for, e.g., the Mediterranean [6], which will also greatly benefit from FOWTs.

According to WindEurope [6], Europe needs 100–150 GW of floating wind energy in order for Europe to reach climate neutrality. At present, nearly 350 MW of FOWTs

are planned to be online by 2022 and more than seven countries in Europe have the ambition to develop their FOWT sector in the next decade [6]. Despite already being a proven technology with 74 MW online, of which 62 MW is located in Europe, FOWT is still challenged by higher LCoE [6]. WindEurope [6] currently estimates the LCoE for floating wind to be ~200 EUR/MWh and predicts that with the technology development, increased sector volume, and government policies, the LCoE will reach 50-65 EUR/MWh by 2030. In comparison, conventional offshore wind was estimated to be in the range of 61–72 EUR/MWh in 2019 [7,8]. In general, both onshore and offshore wind energy have seen an accelerated cost reduction in recent years, reaching a level far below the previously expected value, and is expected to decline further by between 37 and 49% by 2050 [9].

In order for the FOWT technology to reach a fully commercial and economically feasible stage, it is a strategical approach to ensure a design which is ready for a scalable and industrialized production, which minimizes required work at the port of embarkation and which eliminates the need for specialized vessels [10].

The TetraSpar FOWT foundation, as seen in Figure 1, has been designed based on these criteria, solely relying on components that are highly industrialized and suitable for mass production, with an already existing supply chain. The production takes place at factories and the structure is assembled at ports by an already available workforce [10]. A TetraSpar 3.6 MW demonstrator has presently been manufactured and assembled in Denmark, ready for deployment and with expected installation at the Norwegian coast during 2021 [10,11].

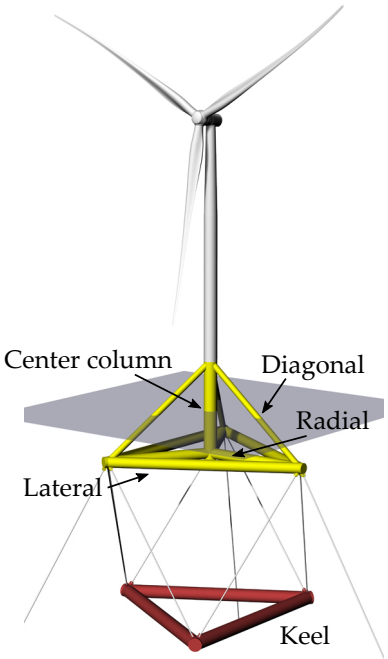

Figure 1. The TetraSpar FOWT foundation concept, with the naming of the various elements.

In addition to the apparent criteria needed for securing commercialization, the floating foundation naturally needs to provide sufficient static and dynamic stability. The TetraSpar foundation has been developed over several years, addressing both commercial and research topics. The latter has been particularly focused on the dynamic response of the concept. Several experimental campaigns have tested the coupled hydro- and aerodynamic response [12–14], while numerical models have been used to test various design aspects and response of the FOWT foundation [15–17].

The present paper investigated and compared the prevalent hydrodynamic models used in the analysis and the investigation of the TetraSpar concept. Traditionally, a Morison model [18] or a linear boundary element method (BEM) [19–22] is used to investigate the loads on an offshore structure, therefore forming the basis of this study. These modelling

approaches are recommended in most design standards such as DNVGL-OS-E301 [23], DNVGL-RP-C205 [24], IEC TS 61400-3-2:2019 [25] and DNVGL-ST-0119 [26]. The applicability of each model is highly dependent on the structure size and sea states, since the Morison approach is applicable on slender structures, while the BEM approach should be considered for larger structures where diffraction is dominant. The following sections will describe the models in more detail. The different models were tested and investigated widely, and combined into hybrid models in, e.g., [27] in order to include most hydrodynamic effects. However, many higher order effects and phenomena such as wave slamming are not included and need even more sophisticated models such as traditional CFD (computational fluid dynamics) or SPH (smoothed particle hydrodynamics). This paper will present the limitations of the Morison, BEM and hybrid models when investigating the motion response of a FOWT and highlight the influence from various design choices. The paper will focus on sea states relevant for the TetraSpar FOWT foundation, and investigate the applicability of the different models on structures such as the TetraSpar.

The paper is structured with this introduction, followed by a description of the models and cases. Section 3 presents, compares and discusses the results and is followed by the concluding remarks. A more detailed description of the TetraSpar and its structure can be found in [10].

2. Methodology

The TetraSpar FOWT foundation consists of 10 cylinders connected in the tetrahedral shape illustrated in Figure 1. The figure also presents the naming of each element, while Table 1 lists each of their corresponding diameters. The floating foundation is moored to the seabed through three catenary lines composed of chain, rope and clump weights. The system was designed to provide sufficient restoring force and natural frequencies well below the investigated wave frequencies. More details on the structure and properties, together with mooring parameters, can be found in [10].

Table 1. Definition of diameters of the foundation elements.

Element	Diameter (m)
Center column	4.3
Lateral	4.1
Radial	3.5
Diagonal	2.0
Keel	4.3

For a complete design of the foundation, both operational and extreme conditions are considered. While the operational conditions are more prevalent in the fatigue limit state (FLS), the extreme events are often determined for mooring and power cable design (maximum surge motions), together with rotor nacelle assembly (RNA) limits such as maximum pitch and accelerations. The design cases have been selected based on expected conditions for the deployment site of the TetraSpar foundations, and cover six operational and four extreme cases, cf. Table 2. All waves are modelled as long crested 2D waves with a Torsethaugen spectrum and a duration of three hours. Only one wave direction is considered in the present study, aligned with one of the mooring lines.

2.1. Time Domain Solver: The OrcaFlex Software Package

For the simulation of the time domain response of a floating structure, many different commercial software packages and in-house codes are available. One of the most widely applied commercial tools is the OrcaFlex software package by Orcina [28,29]. The software package is capable of solving the equations of motions (EoMs) and includes effects from environmental loads, moorings and structural properties.

When solving the time domain response of the hydrodynamic loads, OrcaFlex applies either a Morison or a BEM approach. The following subsections briefly present the different approaches.

Table 2. Definition of environmental conditions for the 10 cases.

Case	Significant Wave Height, H_s (m)	Peak Wave Period, T_p (s)	Peak Wave Length, L_p (m)	Water Depth, h_d (m)
Operational, O1	0.4	3.40	18.1	220.0
Operational, O2	1.8	6.8	72.3	220.0
Operational, O3	2.5	7.8	94.4	220.0
Operational, O4	3.6	9.1	129.4	220.0
Operational, O5	5.7	10.9	185.7	220.0
Operational, O6	8.0	12.5	244.2	220.0
Extreme, E1	9.3	13.9	302.0	220.0
Extreme, E2	11.4	15.1	356.4	220.0
Extreme, E3	12.9	16.0	400.1	220.0
Extreme, E4	16.3	18.0	506.4	220.0

2.2. Morison Approach

In the Morison approach, the time varying loads are solved using the Morison equation (Equation (1)) [18]. The equation is valid for slender structures, where the nominal width (D) is small compared to the incoming wavelength. Hence, the presence of the body only results in negligible interference with the surrounding wave field. The load can, therefore, be expressed as a combination of a contribution from inertia and from drag:

$$F_{Morison} = \underbrace{\rho\, C_m\, V\, \dot{u}}_{F_I} + \underbrace{\frac{1}{2}\,\rho\, C_D\, A\, u\, |u|}_{F_D} \tag{1}$$

where ρ is the fluid density, C_m is the inertia coefficient ($C_m = 1 + C_a$, with C_a being the added mass coefficient), V is the submerged volume of the body, $\dot{u}$ is the fluid acceleration, C_D is the drag coefficient, A is the reference area and u is the fluid velocity. F_I and F_D correspond to, respectively, the inertia and drag force contribution.

The inertia, drag and added mass coefficients can either be found from experimental test or, e.g., CFD (computational fluid dynamics), but also found in design standard or literature such as DNVGL-RP-C205 [24]. The chosen conservative values are defined in Table 3, based on standard values. The same values are applied for all elements in the structure and for all sea states. This choice will be discussed and investigated later in the paper.

Table 3. Coefficients used in the Morison approach.

Coefficient	Value
C_D	1.05
C_a	1.0
C_m	2.0

In OrcaFlex, the TetraSpar foundation is modelled as a number of object (defined as *"Spar Buoys"* in OrcaFlex), for which the equation is solved. Based on the loads and mooring system, the time domain response of the coupled behaviour of the system is simulated. The approach accounts for several contributions all presented in Table 4 and described further in Section 2.4.1.

2.3. Boundary Element Method (BEM) Approach

The BEM is based on linear potential theory, assuming linear waves with low steepness, while also assuming small amplitude of motions of the floating body. The method is valid for large structures and takes into account wave radiation, diffraction and inertia loads. The BEM model does not account for any viscous effects [19–22,30].

First, the hydrodynamic coefficents are solved in a BEM code such as WAMIT [22], OrcaWave [31] or Nemoh [30], with the first being used for this study. The frequency dependent hydrodynamic coefficients are imported into OrcaFlex (defined as a "*Vessel*" object), and the Cummin's Equation is used to model the time domain behaviour [32]. Based on the BEM solver, both the first and second order wave effects can be taken into account. OrcaFlex allows for use of Quadratic Transfer Functions (QTFs) for second order effects but also the use of the more simple Newmann Approximation, which solves the second order effects based on first order quantities [33].

2.4. Hybrid Modelling

As presented in the two previous subsections, the Morison approach is primarily valid for slender structures, while the BEM approach is valid for larger structures. Both approaches have limitations, e.g., Morison does not account for diffraction/radiation, while BEM does not account for viscous drag.

As illustrated in Figure 2, different load regimes are dominant for the different components of the TetraSpar. The most slender elements (the diagonals) are mostly dominated by inertia and drag, even for the operational sea states, which have the shortest wavelengths. For the largest element (the centre column), drag is not as dominant, and most sea states are expected to be dominated by the inertia load contribution. For the smallest sea states, diffraction is dominating. The values in the diagram are based on H_s and L_p, meaning that even smaller waves will be present in each sea state, which will result in even more waves in the diffraction region.

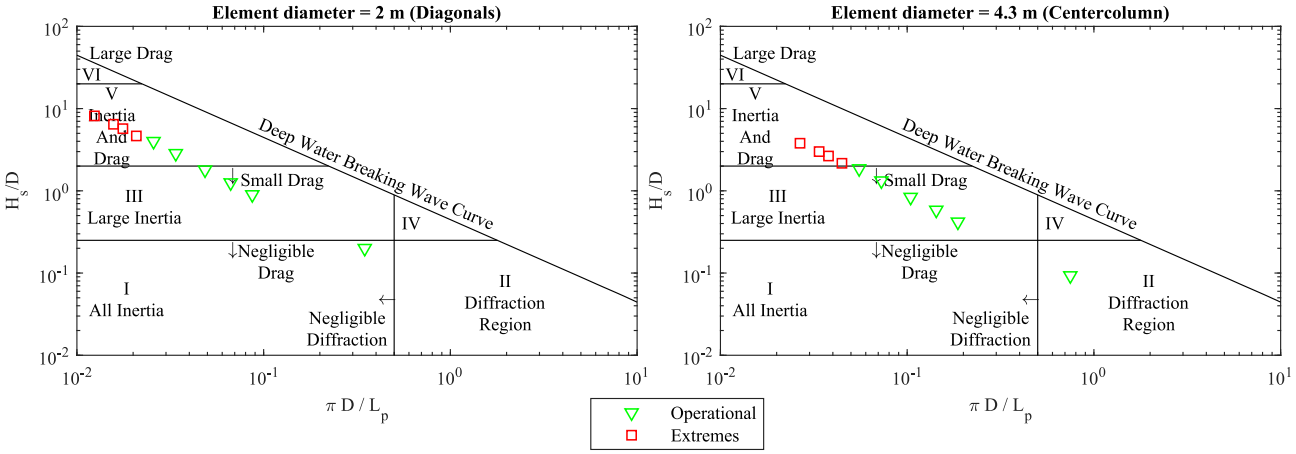

Figure 2. Sea states plotted against the dominating load regimes as defined in [20,34] for the most slender element (**left**) and the largest (**right**).

In order to account for the combined effects, hybrid models have been introduced in studies such as [27]. This type of model combines the BEM approach and the Morison approach to account for more effects. The model takes its basis in the BEM approach and uses all the quantities from this, while also adding the Morison drag contribution. The inertia coefficient from the Morison approach is not included in order to limit the doubling of inertia effects. By implementing this approach, dominant effects such as viscous damping are included within the BEM model. The importance of this was highlighted in [27].

2.4.1. Model Comparison

In the time domain simulation of the motion response, the following EoM is solved:

$$M(p,a) + C(p,v) + K(p) = F(p,v,t) \quad (2)$$

where $M(p,a)$ is the inertia load, $C(p,v)$ is the damping load, $K(p)$ is the stiffness load and $F(p,v,t)$ is the external load. p, v and a are the position, velocity and acceleration, respectively, while t is the simulation time.

The different modelling approaches primarily affect inertia, damping and external loads, while stiffnesses are similar among the models. For all types of modelling approaches in this study, non-linear hydrostatic stiffness is applied and the same mooring system is considered.

A comparison of the modelling of the different contributions in the three approaches is presented in Table 4.

Table 4. Comparison of the included effects in each modelling approach.

	Morison Approach		BEM Approach		Hybrid Approach	
Inertia						
Froude–Krylov	✓	Instantaneous submerged volume	✓	Freq. dependent $C_{FK}(\omega)$	✓	Freq. dependent $C_{FK}(\omega)$
Added mass	✓	Constant C_a	✓	Freq. dependent $C_A(\omega)$	✓	Freq. dependent $C_A(\omega)$
Diffraction	✗		✓	Freq. dependent $C_{diff}(\omega)$	✓	Freq. dependent $C_{diff}(\omega)$
Radiation	✗		✓	Freq. dependent $C_r(\omega)$	✓	Freq. dependent $C_r(\omega)$
Drag	✓	Constant C_D Scaled to wet area	✗		✓	Constant C_D Scaled to wet area
Damping						
Linear	✓	Constant, $C_{d,l}$	✓	Freq. dependent radiation damping $C_r(\omega)$	✓	Freq. dependent radiation damping $C_r(\omega)$
Quadratic	✓	Viscous damping from C_D	✗		✓	Viscous damping from C_D
Wave drift damping	✓	From motion response	✓	From QTF	✓	From QTF and motion response
Wave Drift	✓	From C_D and C_M with instantaneous area and displaced volume Non-linear waves	✓	From QTF	✓	From QTF and C_D, instantaneous area and non-linear waves
Stiffness	✓	Non-linear hydrostatic stiffness	✓	Non-linear hydrostatic stiffness	✓	Non-linear hydrostatic stiffness

The inertia load in all cases includes the Froude–Krylov force results from the undisturbed pressure field around the body [20]. For the BEM and hybrid approaches, this contribution is included as a frequency-dependent coefficient, while in the Morison approach, OrcaFlex estimates the force contribution from the wave kinematics and the instantaneous submerged volume [29]. For large waves and body motions, this approach is therefore expected to provide a better estimate, since the BEM cannot take this into account due to its assumptions.

Similarly, the added mass contribution is included in all approaches. For the Morison approach, the contribution is included through a constant coefficient C_a, while the BEM and hybrid model include frequency-dependent coefficients.

Diffraction and radiation are only included in the BEM and hybrid model as frequency dependent coefficients.

The BEM model does not in itself include any viscous effects, and hence does not provide any drag contribution. In the Morison approach, the drag contribution, as seen from Equation (1), is included by use of a constant coefficient C_D.

The BEM solves the linear radiation damping coefficients, which are also included in the hybrid model. The Morison approach in OrcaFlex also allows for the specification of a linear damping coefficient, which, however, was not considered in this study because experimental data would be needed for tuning.

The quadratic viscous damping contribution arises from the drag, and hence in the Morison and hybrid models, this contribution is included. Due to the lack of viscous effects in the BEM model, no quadratic damping is present.

Wave drift damping arises from the second order low-frequency motions of the body in the waves [35]. The BEM approach in OrcaFlex includes this effect by use of the QTF or the Newman method [33]. In the Morison approach, the motion response of the structure and the earlier mentioned coefficients result in some damping. Since the hybrid model includes both the QTF term from the BEM approach and the drag coefficient from the Morison approach, some doubling effect could potentially occur.

All three modelling approaches will result in a constant drift of the structure. In the BEM approach, OrcaFlex uses the QTFs to model the effect, while the Morison approach experience the drift due to several phenomena. Figure 3 shows how the non-linear waves result in a larger fluid particle velocity at the wave crest compared to the velocity at the trough. The drag force will, therefore, be larger when the wave crest passes the body, compared to when the wave trough passes, also due to the fact that OrcaFlex accounts for the instantaneous wetted area when calculating the total force. Consequently, a constant drift in the wave direction will be seen. Similarly, since the Froude–Krylov is related to the instantaneous submerged volume, non-linear waves result in a constant drift of the body.

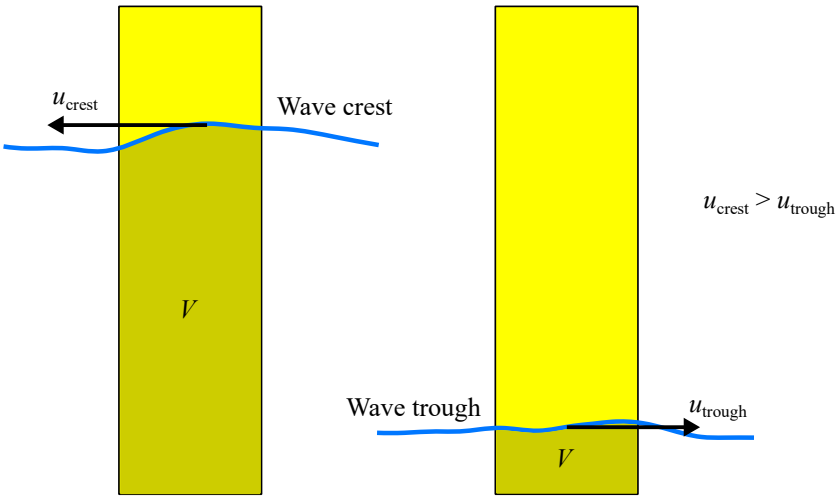

Figure 3. Illustration of the difference in wave velocities over the surface-piercing elements. V indicates the submerged volume.

2.5. Comparing the Modelling Approaches

In order to compare the three models, the sea states defined in Table 2 are simulated as three hour time series and the resulting motion responses are compared. The following section presents the results and discusses the influence of various parameters and relevant changes to some of the input parameters.

3. Results

In order to evaluate the response in each sea state for the three models, the most probable maximum (MPM) is considered. In design standards such as DNVGL-OS-E301 [23], this value is characterized as the design value for, e.g., mooring line tension. The MPM value is calculated from:

$$MPM = \mu + \sigma\sqrt{2\ln n} \tag{3}$$

where μ is the mean value, σ is the standard deviation and $n = T/T_z$ is the number of peaks in the time series ($T = 3$ h is the time series duration and T_z is the mean up-crossing period of the respective response).

Figure 4 presents the mean value of the surge displacement, which corresponds to the mean wave drift value. As expected, the larger wavelengths (indicating the more extreme sea states) result in larger mean displacements. Clearly, the BEM approach provides a significantly lower value compared to the hybrid and Morison approaches. This deviation increases with the wavelength and is primarily explained by the lack of drag loads in this model. Considering Figure 2, this corresponds well with the fact that the larger sea states are in the inertia and drag domain. The larger sea states are more non-linear than the smaller sea states, and hence, the water particle velocity in the wave crest is larger than in the wave trough (cf. Figure 3). This affects the drag-induced loads and this effect is captured by both the hybrid and Morison model.

From Figure 4, it can also be seen that the Morison approach provides lower values than the hybrid approach for the smaller sea states, but larger results for the more extreme ones. Since the drag coefficients for these two models are identical, the main difference is in the inertia loads. From Table 4 it is seen that the inertia loads in the Morison approach account for the instantaneously displaced volume, which will mostly vary in the extreme cases. Under operational conditions, drag is of less importance (cf. Figure 2), meaning that the larger mean drift in the hybrid approach compared to the Morison arises from differences in the included inertia and damping. Since the hybrid model accounts for diffraction, this contribution might be of more importance under these conditions, while the larger linear damping in the hybrid model from radiation might also induce larger mean drift. The hybrid approach is based on the linear theory, with low steepness waves and small amplitude motions. Consequently, larger inertia loads can be expected in the Morison approach.

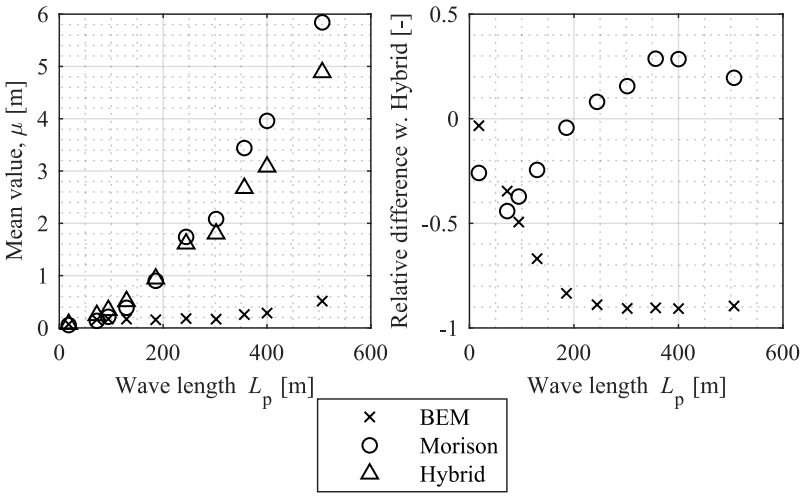

Figure 4. Mean value, μ, of the surge displacement, corresponding to the mean wave drift (**left**). The **right** figure illustrates the relative difference with the hybrid model.

Observing Figure 5, the standard deviation of motion results for three degrees of freedom (DoFs) is shown: surge, heave and pitch. When considering the surge DoF, similar tendencies are observed among the three models. For most cases, the BEM provides larger standard deviation values, which to some extent can be explained from the much smaller drift motion seen in Figure 4. When the system is less excursed, the restoring mooring stiffness is much smaller, meaning that the body is expected to be more dynamic and experience larger oscillations around the mean position.

It is evident that the smallest sea state provides a larger value for both the Morison and BEM approaches compared to the hybrid model. Since the hybrid and Morison model both have the same drag coefficient, some of the difference must be explained by the different treatment of inertia loads. Furthermore, the drag coefficient will affect this result.

For the heave motion, the BEM and Morison approaches provide the largest results in almost all cases. Again, the larger motions in the BEM model can be explained by a lower mean drift. Since the hybrid model experiences more drag for the larger sea states where drag becomes more dominant, the difference between these two models decreases. The Morison model still experiences larger loads from the inertia coefficient, meaning larger values compared to the hybrid model.

For the pitch DoF, the BEM and hybrid models are relatively similar, indicating a small influence from drag on this DoF, while the Morison approach has a tendency to provide smaller values, probably because the inertia coefficient in the Morison model only results in minor pitch motion, and does not take into account the same effects as the hybrid and BEM model.

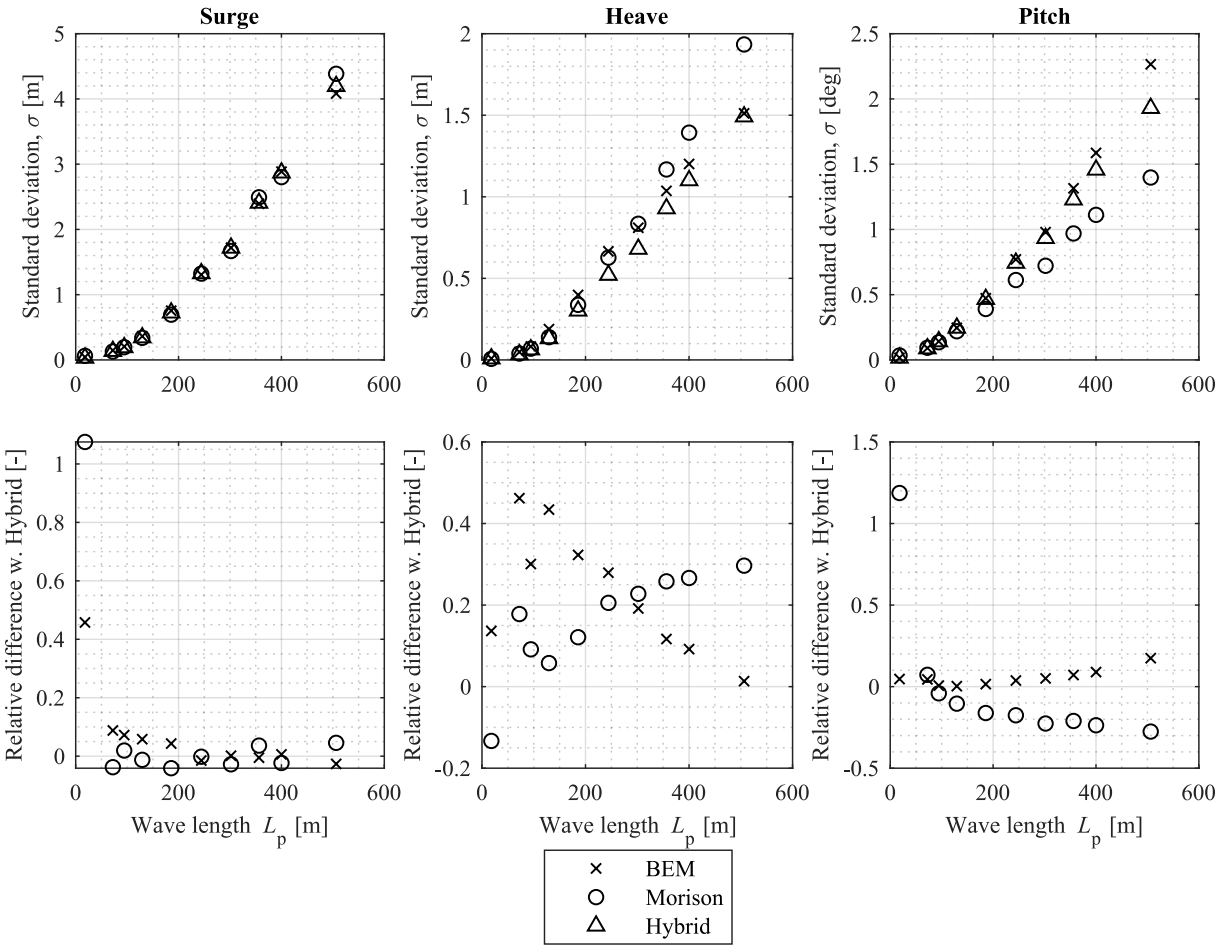

Figure 5. Top: Standard deviation, σ of the surge (**left**), heave (**middle**) and pitch (**right**) DoF. The bottom figures illustrates the relative difference with the hybrid model.

The *MPM* values presented in Figure 6 are a result of the parameters in Figures 4 and 5 (cf. Equation (3)). However, since it is considered a design value, it is relevant to consider. The BEM approach tends to provide less surge motion than the hybrid and Morison approaches, while it provides more in heave and pitch. The Morison approach results in the largest surge motions, but is smaller in heave (though approaches the same value for larger sea states) and particularly in pitch.

From the MPM results, it is evident that the standard deviation provides a large influence on the design value. Considering Equation (3), this is explained by the factor $\sqrt{2\ln n}$. When there are large values of standard deviation, the design value increases significantly. This also affects the relative difference between the models. Because of the relatively good agreement between the standard deviations, the difference between MPM values decreases. This is seen in Figure 6, where, e.g., the difference between MPM is between -20% and $+10\%$ for Morison and between -5% and -20% for the BEM. The standard deviation provides differences of less than 10% in most cases (except the smallest sea states where differences of up to 100% are present), while the mean surge shows differences of up to 90% for BEM and up to 40% for the Morison. This clearly indicates the importance of the standard deviation on the design MPM value.

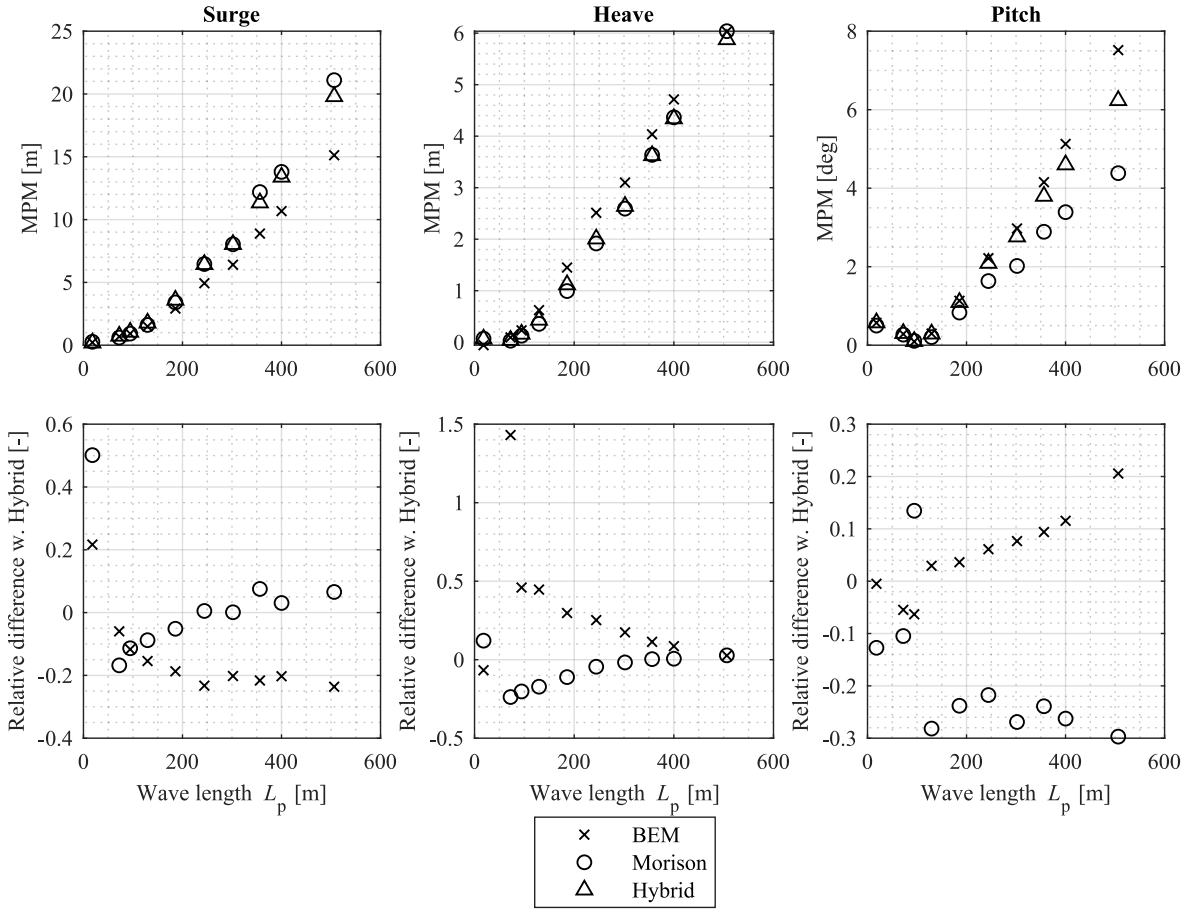

Figure 6. Top: Most probable maximum, *MPM* of the surge (**left**), heave (**middle**) and pitch (**right**) DoF. The bottom figures illustrate the relative difference with the hybrid model.

From the previous figures, it is clear that the drag and inertia coefficients are highly influencing the motions of the TetraSpar FOWT. Since no experimental data are available, it is challenging to actually quantify which model provides the most reliable results. Due to the high influence from drag seen in the results, it is, however, relevant to consider it further.

The drag coefficient is dependent on the Reynolds number, Re, defined in Equation (4) [24]:

$$Re = \frac{\rho\, u\, L}{\mu_d} \tag{4}$$

where L is the characteristic linear dimension, u is the relative flow velocity and μ_d is the dynamic viscosity. The drag is dependent on both the dimensions of each element of the TetraSpar and also the given sea state. The drag coefficient will not only vary for all elements due to the variation in diameter (cf. Table 1), but will also vary for each sea states due to the variations in wave kinematics and body motions, cf. Figure 7. Even within each sea state, the drag coefficient will vary as a result of the irregular nature of the waves. In Table 5, new drag coefficients are presented, taking into account the element diameter and the wave particle velocity in a corresponding regular wave with wave height and period similar to the H_s and T_p of the different sea states. Clearly, significantly lower values can be applied compared to the initial value.

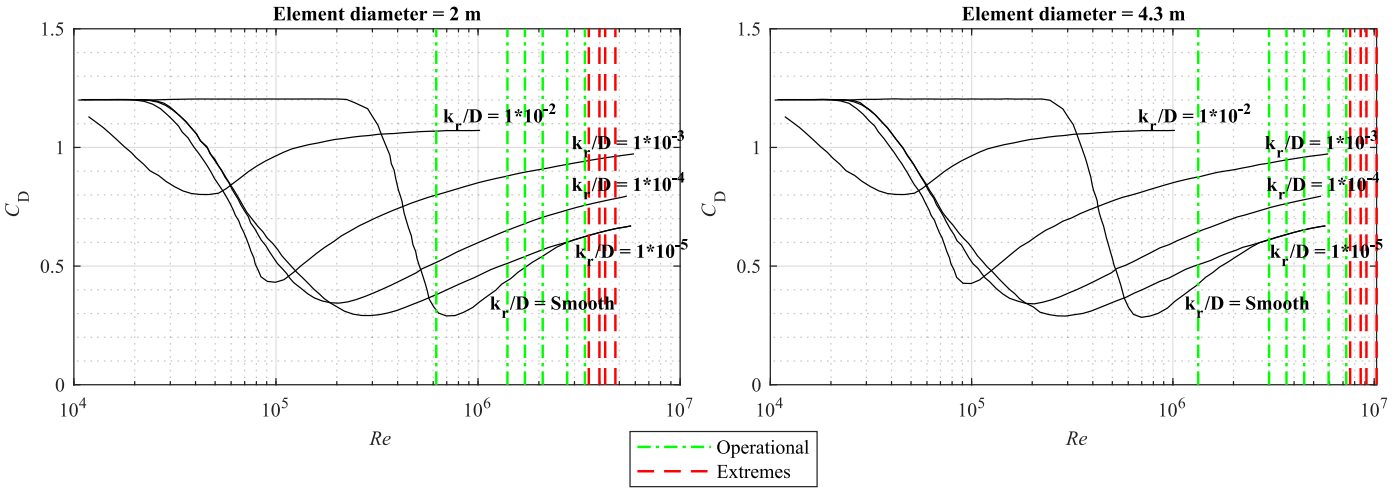

Figure 7. Drag coefficients as a function of the Reynolds number as defined in [24] for the largest (**right**) and smallest (**left**) diameter. The dotted lines indicates the sea states.

Table 5. Updated drag coefficients applied for each element of the TetraSpar in the investigated sea states.

Component	O1	O2	O3	O4	O5	O6	E1	E2	E3	E4
Center column	0.42	0.60	0.63	0.65	0.67	0.67	0.67	0.67	0.67	0.67
Lateral	0.40	0.60	0.62	0.65	0.67	0.67	0.67	0.67	0.67	0.67
Radial	0.30	0.50	0.55	0.60	0.65	0.65	0.67	0.67	0.67	0.67
Diagonal	0.30	0.45	0.50	0.55	0.60	0.62	0.62	0.65	0.65	0.65
Original value (all elements)	1.05									

Figure 8 presents the mean value of the surge motion with the updated drag coefficients from Table 5. When comparing to the original figure, it is clearly observed that the mean wave drift is significantly reduced due to the lower drag loads on the structure. For the most extreme case, where the drag contribution is large, a reduction of approximately 25% on the mean wave drift is achieved. The difference between the BEM and hybrid model appears to have decreased slightly from a maximum of 90% to 85%, while the difference between the Morison and the hybrid model has increased from a maximum of 30% to 40%. Since the hybrid model experiences wave drift from both the QTF and drag contributions, the reduction in the drag coefficient possibly reduces the double effect, and

hence the reduction in drift in this model is largest, reducing the differences with the BEM and increasing the differences with the Morison.

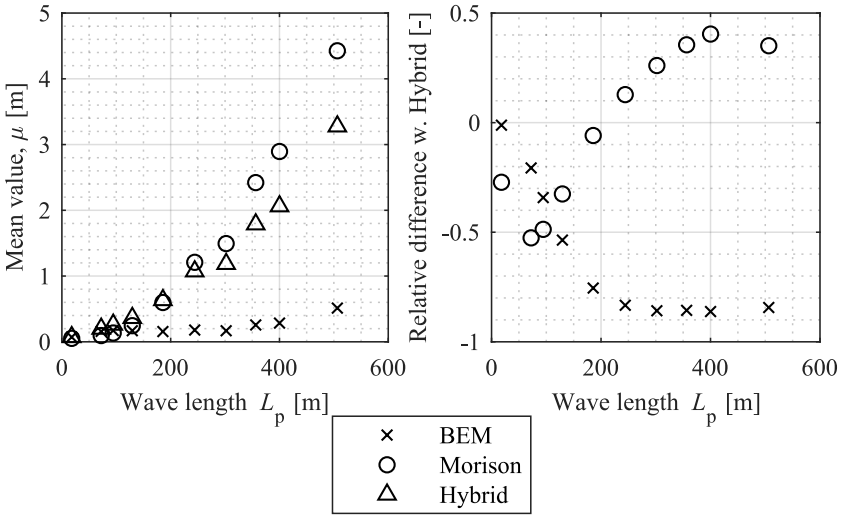

Figure 8. Mean value, μ, of the surge displacement with updated drag coefficients (**left**). The **right** figure illustrates the relative difference with the hybrid model.

Comparing the standard deviation in Figure 9 of all the motion response of the three investigated DoFs, a more outspoken reduction in differences is seen. The heave DoF presents the same tendencies as before but the difference between the models has been reduced from a maximum difference of 45% to approximately 35%. The reduction is largest for the BEM model. A similar tendency can be observed for the pitch DoF. Here, the BEM and hybrid approaches are very similar, while the Morison model still provides less motion response. The surge DoF is significantly improved with approximately 10% difference between the models in almost all sea states.

The agreement between the models indicates that the previous models most likely caused overly large drag loads, resulting in the larger response. Since the mean surge drift is now smaller, the induced loads from the mooring is also smaller and the stiffness lower, also causing the oscillations of all DoF to be more similar between the models.

As a consequence of the results in Figures 8 and 9, the *MPM* results also present a smaller difference between the three models compared to the original. This is observed in all three DoFs.

Observing the relative difference of the surge motion in Figure 10, it is clear that the Morison model provides larger values for the sea states with the shortest wavelengths, compared to all the other models.

In the same way as for the drag coefficient, the dimensions of the elements in the TetraSpar FOWT also determine the numerical value of the inertia coefficient. The value also varies in the different sea states. Figure 11 illustrates C_m for the largest and the most slender elements. The dotted lines indicate the investigated sea states. In most conditions, the assumption of $C_m = 2$ is valid, but the smallest sea state (O1) results in a lower C_m-coefficient for the largest element (the centre column) going from $C_m = 2$ to $C_m = 1.7$.

Changing the C_m coefficient only affects the Morison approach. The change is only done for the centre column and only for the O1 sea state. Table 6 presents the influence of the updated C_m-coefficient on the surge motion.

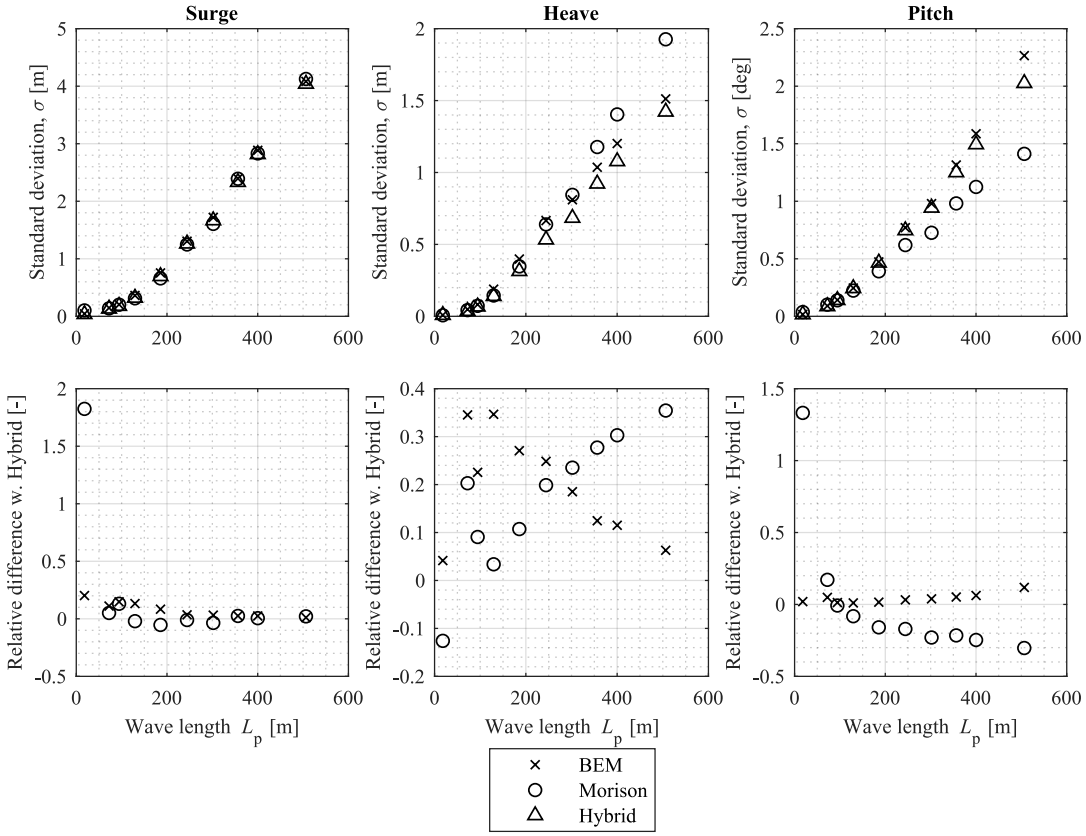

Figure 9. Top: Standard deviation, σ, of the surge (**left**), heave (**middle**) and pitch (**right**) DoF with updated drag coefficients. The bottom figures illustrates the relative difference with the hybrid model.

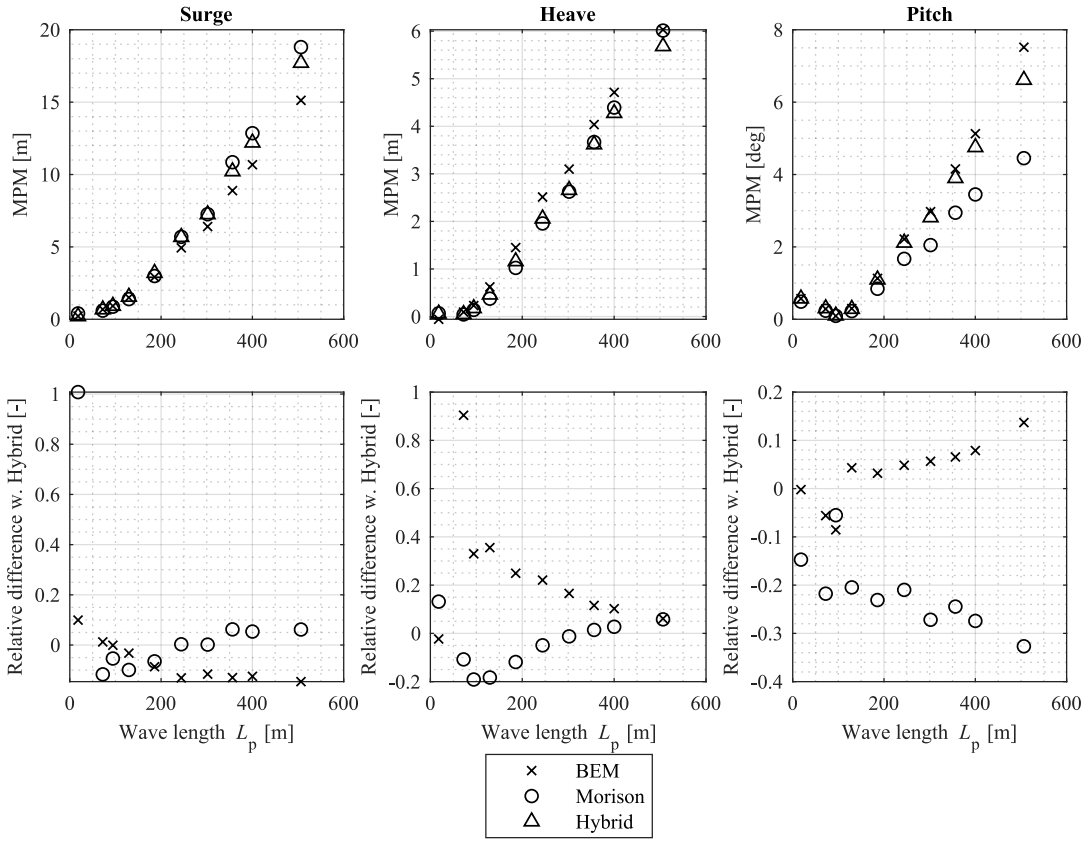

Figure 10. Top: Most probable maximum, *MPM* of the surge (**left**), heave (**middle**) and pitch (**right**) DoF with updated drag coefficients. The bottom figures illustrate the relative difference with the hybrid model.

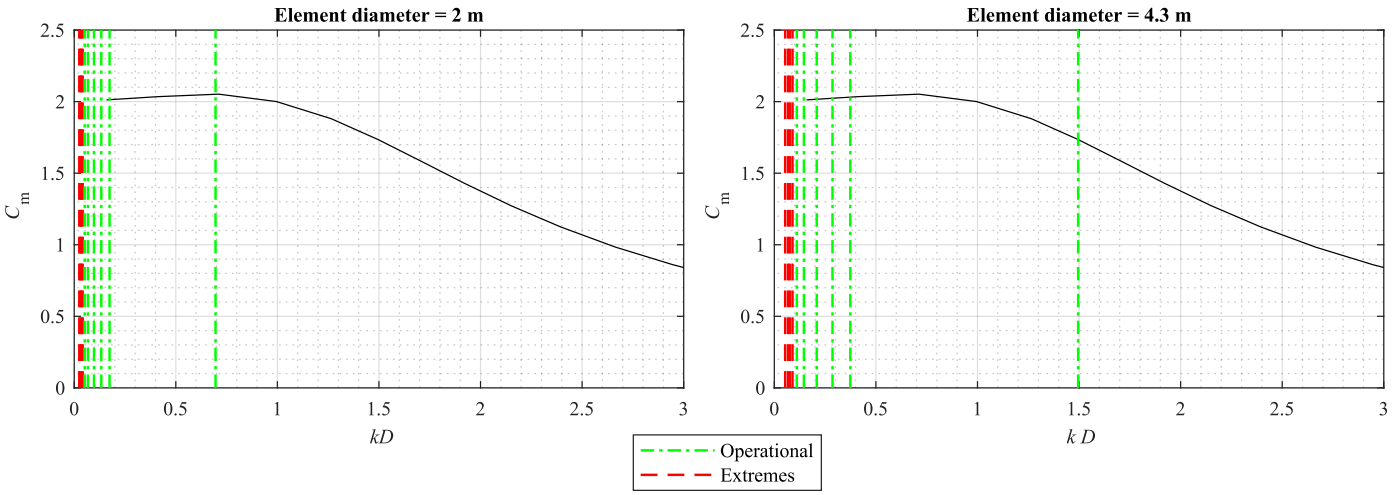

Figure 11. Inertia coefficients, as defined in [24], for the smallest (**left**) and largest (**right**) element in the TetraSpar.

Table 6. Surge motion response for the three models with and without improved C_m. The relative difference is with the hybrid approach.

	Morison						
	Original C_m		Updated C_m		BEM		Hybrid
Parameter	**Value**	**Rel. diff.**	**Value**	**Rel. diff.**	**Value**	**Rel. diff.**	**Value**
μ (m)	0.052	0.72	0.052	0.72	0.071	0.99	0.072
σ (m)	0.103	2.86	0.070	1.94	0.044	1.22	0.036
MPM (m)	0.404	2.02	0.294	1.47	0.222	1.11	0.200

The motion response decreases with a reduced inertia coefficient, resulting in a smaller difference between the approaches. In sea state O1, the diffraction and radiation (cf. Figure 2) are dominant, meaning that the C_m value might not be applicable to this sea state. The presence of radiation damping could potentially reduce the response even further, and might explain the difference between the models in this sea state.

4. Discussion and Concluding Remarks

The present study investigated three different approaches for hydrodynamic modelling of the motion responses of the TetraSpar FOWT foundation concept: a Morison, a BEM and a hybrid approach. This study illustrated some of the differences between the models and how these affected the motion responses. Mean surge motions were particularly affected by the model choice, however, some differences were observed in all DoFs. This results from both the chosen hydrodynamic coefficients but also how the time domain solver handles time varying submerged volume and the exposed drag area. Since the results presented in this study have not been validated with experimental data, it is not possible to quantify the reliability of any of the models, but in most design cases, a conservative choice would be preferable. However, large motions (and corresponding larger loads) also imply a larger cost of mooring, power cables and structure. Since design standards require additional safety factors, a final design would require experimental data to identify the most reliable model, and ensure that the cost does not increase unnecessarily. Considering the eminent desire to reduce LCoE and utilize experience to improve reliability and costs, applying experimental data in order to identify the best modelling approach is highly relevant.

This study illustrated the importance of the inertia C_m and drag C_D coefficients. Since some sea states and wave components are drag dominated, while others are affected by diffraction/radiation, a hybrid model would be desirable. In the hybrid model used in this study, both the diffraction and radiation effects are considered while also accounting for

the drag contribution. Drag coefficients should be specified according to the given sea state. In the Morison approach in this study, the C_m contribution was scaled according to the instantaneous submerged volume, which is not the case for the linear inertia contribution from the BEM model. Combining the BEM and C_m coefficient could possibly be a benefit, but would require experimental data for adjusting the coefficients. In this study, only C_m was investigated, while, naturally, also the added mass coefficient C_a could be relevant to investigate and optimize in future models.

Clearly, experimental data are critical and needed in order to validate and tune the models. Nevertheless, by improving the fidelity of input parameters, the difference between the models decreases. For future studies and investigations, the inclusion of currents and wind loads could also prove a paramount influence and significantly change the response of the structure and performance of the models.

Author Contributions: Conceptualization, J.B.T.; methodology, J.B.T. and H.S.; formal analysis, J.B.T.; investigation, J.B.T.; writing—original draft, J.B.T.; writing—review and editing, A.T., J.B.T. and H.S. All authors have read and agreed to the published version of the manuscript.

Funding: This research was funded by the Energy Technology Development and Demonstration Program (EUDP) through the project "TetraSpar" (Grant number 64017-05171).

Institutional Review Board Statement: Not applicable.

Informed Consent Statement: Not applicable.

Data Availability Statement: Not applicable.

Conflicts of Interest: The authors declare no conflict of interest.

References

1. IRENA. *Future of Wind-Deployment, Investment, Technology, Grid Integration and Socio-Economic Aspects;* International Renewable Energy Agency (IRENA): Abu Dhabi, United Arab Emirates, 2019.
2. IRENA. *World Energy Transistion Outlook-1.5 °C Pathway*; International Renewable Energy Agency (IRENA): Abu Dhabi, United Arab Emirates, 2021.
3. Wind Europe. *Our Energy, Our Future*; Wind Europe: Brussels, Belgium, 2019.
4. BloombergNEF. *New Energy Outlook 2020-Executive Summary*; BloombergNEF: London, UK, 2020.
5. Wind Europe. *Offshore Wind in Europe–Key Trends and Statistics 2018*; Wind Europe: Brussels, Belgium, 2019.
6. Wind Europe. *Floating Offshore Wind*; Wind Europe: Brussels, Belgium, 2020.
7. IRENA. *Renewable Power Generation Costs in 2019*; International Renewable Energy Agency (IRENA): Abu Dhabi, United Arab Emirates, 2020.
8. Rsted, O. *Making Green Energy Affordable-How the Offshore Wind Energy Industry Matured and What We Can Learn From It*; Ørsted: Fredericia, Denmark, 2019.
9. Wiser, R.; Rand, J.; Seel, J.; Beiter, P.; Baker, E.; Lantz, E.; Gilman, P. Expert elicitation survey predicts 37% to 49% declines in wind energy costs by 2050. *Nat. Energy* **2021**, *6*, 555–565. [CrossRef]
10. Borg, M.; Jensen, M.W.; Urquhart, S.; Andersen, M.T.; Thomsen, J.B.; Stiesdal, H. Technical Definition of the TetraSpar Demonstrator Floating Wind Turbine Foundation. *Energies* **2020**, *13*, 4911. [CrossRef]
11. Stiesdal. The TetraSpar Full-Scale Demonstration Project. 2021. Available online: https://www.stiesdal.com/offshore-technologies/the-tetraspar-full-scale-demonstration-project/ (accessed on 5 May 2021).
12. Borg, M.; Viselli, A.; Allen, C.K.; Fowler, M.; Sigshøj, C.; Grech La Rosa, A.; Andersen, M.T.; Stiesdal, H. Physical Model Testing of the TetraSpar Demo Floating Wind Turbine Prototype. In Proceedings of the ASME 2019 2nd International Offshore Wind Technical Conference (IOWTC), Saint Julian's, Malta, 3–6 November 2019; American Society of Mechanical Engineers Digital Collection: New York, NY, USA, 2019.
13. Bredmose, H.; Borg, M.; Pegalajar-Jurado, A.; Nielsen, T.R.; Madsen, F.J.; Lomholt, A.K.; Mikkelsen, R.; Mirzaei, M. *TetraSpar Floating Wind Turbine Scale Model Testing Summary Report*; Technical Report forINNWIND.EU; DTU: Roskilde, Denmark, 2017; Volume 1.
14. Thomsen, J.B.; Têtu, A.; Andersen, M.T. *Experimental Testing of the TetraSpar in Towing and Installation Configuration*; Department of the Built Environment: Aalborg, Denmark, 2020.
15. Pereyra, B.T.; Jiang, Z.; Gao, Z.; Andersen, M.T.; Stiesdal, H. Parametric study of a counter weight suspension system for the tetraspar floating wind turbine. In Proceedings of the International Offshore Wind Technical Conference (IOWTC), San Francisco, CA, USA, 4–8 November 2018; American Society of Mechanical Engineers: New York, NY, USA, 2018; Volume 51975, p. V001T01A003.

16. Pegalajar-Jurado, A.; Madsen, F.J.; Bredmose, H. Damping Identification of the TetraSpar Floater in Two Configurations With Operational Modal Analysis. In Proceedings of the International Offshore Wind Technical Conference (IOWTC), Saint Julian's, Malta, 3–6 November 2019; American Society of Mechanical Engineers: New York, NY, USA, 2019; Volume 59353, p. V001T01A024.
17. Bach-Gansmo, M.T.; Garvik, S.K.; Thomsen, J.B.; Andersen, M.T. Parametric Study of a Taut Compliant Mooring System for a FOWT Compared to a Catenary Mooring. *J. Mar. Sci. Eng.* **2020**, *8*, 431. [CrossRef]
18. Morison, J.R.; Johnson, J.W.; Schaaf, S.A. The force exerted by surface waves on piles. *J. Pet. Technol.* **1950**, *2*, 149–154. [CrossRef]
19. Newman, J.N. *Marine Hydrodynamics*; MIT Press: Cambridge, MA, USA, 1977.
20. Faltinsen, O. *Sea Loads on Ships and Offshore Structures*; Cambridge University Press: Cambridge, MA, USA, 1993; Volume 1.
21. Falnes, J. *Ocean Waves and Oscillating Systems: Linear Interactions Including Wave-Energy Extraction*; Cambridge University Press: Cambridge, MA, USA, 2002.
22. Lee, C.H.; Newman, J.N. WAMIT User Manual; WAMIT, Inc.: Chestnut Hill, MA, USA, 2006.
23. DNV-GL. *Position Mooring*; DNV-GL Offshore Standard DNVGL-OS-E301; DNV-GL: Høvik, Norway, 2018.
24. DNV-GL. *Environmental Conditions and Environmental Loads*; DNV-GL Recommended Practice DNVGL-RP-C205; DNV-GL: Høvik, Norway, 2010.
25. IEC. *Wind Energy Generation Systems-Part 3-2: Design Requirements for Floating Offshore Wind Turbines*; International Electrotechnical Commission (IEC): Geneva, Switzerland, 2019.
26. DNV-GL. *Floating Wind Turbine Structures*; DNV-GL Offshore Standard DNVGL-ST-0119; DNV-GL: Høvik, Norway, 2018.
27. Thomsen, J.B.; Ferri, F.; Kofoed, J. Validation of a Tool for the Initial Dynamic Design of Mooring Systems for Large Floating Wave Energy Converters. *J. Mar. Sci. Eng.* **2017**, *5*, 45. [CrossRef]
28. Orcina Ltd. Orcina. 2021. Available online: https://https://www.orcina.com/ (accessed on 5 May 2021).
29. Orcina Ltd. *OrcaFlex User Manual*; Orcina Ltd.: Ulverston, UK, 2021.
30. Babarit, A.; Delhommeau, G. Theoretical and numerical aspects of the open source BEM solver NEMOH. In Proceedings of the 11th European Wave and Tidal Energy Conference (EWTEC2015), Nantes, France, 6–11 September 2015.
31. Orcina Ltd. *OrcaWave User Manual*; Orcina Ltd.: Ulverston, UK, 2021.
32. Cummins, W. *The Impulse Response Function and Ship Motions*; Technical Report; David Taylor Model Basin: Washington, DC, USA, 1962.
33. Newman, J. *Second-Order, Slowly-Varying Forces on Vessels in Irregular Waves*; Massachusetts Institute of Technology, MIT Press: Cambridge, MA, USA, 1974.
34. Chakrabarti, S. *Handbook of Offshore Engineering*; Elsevier: Amsterdam, The Netherlands, 2005.
35. Newman, J.N. Wave-drift damping of floating bodies. *J. Fluid Mech.* **1993**, *249*, 241–259. [CrossRef]